AMERICAN SOCIETY FOR MICROBIOLOGY | Applied and Environmental Microbiology®

GEOMICROBIOLOGY

Bioavailability of Mineral-Bound Iron to a Snow Algal-Bacterial Coculture and Implications for Albedo-Altering Snow Algal Blooms

Z. R. Harrold,[a,b]* E. M. Hausrath,[a] A. H. Garcia,[a] A. E. Murray,[b] O. Tschauner,[a] J. A. Raymond,[c] S. Huang[a]

[a]Department of Geoscience, University of Nevada, Las Vegas, Nevada, USA
[b]Division of Earth and Ecosystem Science, Desert Research Institute, Reno, Nevada, USA
[c]School of Life Sciences, University of Nevada, Las Vegas, Nevada, USA

ABSTRACT Snow algae can form large-scale blooms across the snowpack surface and near-surface environments. These pigmented blooms can decrease snow albedo and increase local melt rates, and they may impact the global heat budget and water cycle. Yet, the underlying causes for the geospatial occurrence of these blooms remain unconstrained. One possible factor contributing to snow algal blooms is the presence of mineral dust as a micronutrient source. We investigated the bioavailability of iron (Fe)-bearing minerals, including forsterite (Fo^{90}, $Mg_{1.8}Fe_{0.2}SiO_4$), goethite, smectite, and pyrite as Fe sources for a *Chloromonas brevispina*-bacterial coculture through laboratory-based experimentation. Fo^{90} was capable of stimulating snow algal growth and increased the algal growth rate in otherwise Fe-depleted cocultures. Fo^{90}-bearing systems also exhibited a decrease in the ratio of bacteria to algae compared to those of Fe-depleted conditions, suggesting a shift in microbial community structure. The *C. brevispina* coculture also increased the rate of Fo^{90} dissolution relative to that of an abiotic control. Analysis of 16S rRNA genes in the coculture identified *Gammaproteobacteria*, *Betaproteobacteria*, and *Sphingobacteria*, all of which are commonly found in snow and ice environments. Archaea were not detected. *Collimonas* and *Pseudomonas*, which are known to enhance mineral weathering rates, comprised two of the top eight (>1%) operational taxonomic units (OTUs). These data provide unequivocal evidence that mineral dust can support elevated snow algal growth under otherwise Fe-depleted growth conditions and that snow algal microbial communities can enhance mineral dissolution under these conditions.

IMPORTANCE Fe, a key micronutrient for photosynthetic growth, is necessary to support the formation of high-density snow algal blooms. The laboratory experiments described herein allow for a systematic investigation of the interactions of snow algae, bacteria, and minerals and their ability to mobilize and uptake mineral-bound Fe. Results provide unequivocal and comprehensive evidence that mineral-bound Fe in Fe-bearing Fo^{90} was bioavailable to *Chloromonas brevispina* snow algae within an algal-bacterial coculture. This evidence includes (i) an observed increase in snow algal density and growth rate, (ii) decreased ratios of bacteria to algae in Fo^{90}-containing cultures relative to those of cultures grown under similarly Fe-depleted conditions with no mineral-bound Fe present, and (iii) increased Fo^{90} dissolution rates in the presence of algal-bacterial cocultures relative to those of abiotic mineral controls. These results have important implications for the role of mineral dust in supplying micronutrients to the snow microbiome, which may help support dense snow algal blooms capable of lowering snow albedo and increasing snow melt rates on regional, and possibly global, scales.

KEYWORDS *Chloromonas brevispina*, algal-bacterial coculture, forsterite, iron bioavalibility, mineral weathering, pedobacter, snow algae

Received 23 October 2017 **Accepted** 15 January 2018

Accepted manuscript posted online 26 January 2018

Citation Harrold ZR, Hausrath EM, Garcia AH, Murray AE, Tschauner O, Raymond JA, Huang S. 2018. Bioavailability of mineral-bound iron to a snow algal-bacterial coculture and implications for albedo-altering snow algal blooms. Appl Environ Microbiol 84:e02322-17. https://doi.org/10.1128/AEM.02322-17.

Editor Frank E. Löffler, University of Tennessee and Oak Ridge National Laboratory

Address correspondence to Z. R. Harrold, zoe.harrold@dri.edu, or E. M. Hausrath, Elisabeth.Hausrath@unlv.edu.

* Present address: Z. R. Harrold, Division of Earth and Ecosystem Sciences, Desert Research Institute, Reno, Nevada, USA.

The extent of snow and ice coverage and its high albedo are major factors influencing the global heat budget. While the influence of dust and black carbon accumulation on snow is well studied (e.g., 1), the impact of snow algal blooms on regional and global albedo and heat budgets is poorly understood (2–4). Snow algae include over 110 documented species (5) and are found across myriad permanent and seasonal alpine and continental snow and ice environments during the melt season (2, 3, 5–7). These cryophilic microalgae and associated snow microbiota face numerous environmental stressors, e.g., nutrient limitation, high UV, and subzero temperatures (8). Despite their harsh environment, snow algae can reach high cell densities, with concentrations upwards of 10^6 cells per ml (7). These levels are comparable to *Chlamydomonas* and other green algae in freshwater lake systems that range from 10^2 to 10^6 cells per ml (9).

Snow algal blooms, found in patchy (cm^2) to snowfield scale distributions, span much of the visible spectrum from red to green. Due to their pigmentation and high cell densities, the blooms can lower the albedo of snow and ice by up to 50% (3, 4, 9, 10). Recent work has suggested that this albedo-lowering effect may significantly affect snowmelt rate and the global energy budget (2, 3). These concerns have led researchers to call for the inclusion of pigmented snow algae in numerical albedo models (2, 3). Current understanding of the environmental factors governing the geospatial distribution of snow algae is, however, limited and presents a challenge for predicting and modeling the occurrence of albedo-altering blooms.

Proliferation of snow algae begins during the melt season, when algal zoospores migrate upwards from the snow-soil interface via meltwater within the snowpack and replicate below the snow surface (7). The availability of liquid water is critical to snow algal growth (see, e.g., reference 11) and likely plays an important role in nutrient mobilization, though the sourcing and acquisition of dissolved nutrients by snow algae are not well understood. Studies show little correlation between aqueous geochemical parameters, including major element concentrations, and snow algal biomass content (3). Hamilton and Havig (12) noted enrichment of trace nutrients, including Fe, Mn, and P, in snow algal blooms relative to element ratios in local mineral assemblages, suggesting that algae may have a role in biological sequestration of inorganic nutrients. Microscopic observations of field samples have shown direct associations between snow algae and minerals (13, 14) as well. These results suggest that snow algal growth may be limited in part by the availability, and perhaps bioavailability, of inorganic micronutrients such as Fe and that inorganic trace nutrients may be supplied via mineral dust. Fe bioavailability within snow is of particular interest, since Fe as Fe(III) is sparingly soluble at the pH of snow (pH $\sim$ 5.5) (3, 5), and mineral dust likely provides the largest reservoir of Fe within snow.

Fe is a particularly important micronutrient for photosynthetic organisms, where it is required for chlorophyll production and electron transport during photosynthesis, in addition to other cellular functions, such as respiration and nitrogen assimilation (15, 16). This incorporation of Fe into biomolecules renders the intracellular Fe concentration of photosynthetic microbes 4 to 6 orders of magnitude higher than that of their environment (15). The manifestation of Fe limitation in photosynthetic life can take many forms, including decreased cell concentrations and growth rates, changes in phenotype such as cell size, a decrease in photosynthetic efficiency, and a dearth of photosynthetic pigment production known as chlorosis (16). In Fe-limited marine systems, the addition of Fe has been shown to stimulate plankton assemblages, resulting in increased growth of phytoplankton relative to bacteria (16–18). In addition, Fe has been shown to be colimiting with N and P in freshwater systems (19) and is suspected to be important in snow (12), though further work is needed to better understand Fe in natural snow systems.

Microalgal-bacterial partnerships have been shown to play a role in nutrient acquisition (for examples, see references 20, 21, and 22), including the provision of bioavailable Fe to algae (23, 24). Bacteria are known to selectively colonize and enhance the dissolution of minerals that contain micronutrients such as Fe (25–29). Bacterial Fe

TABLE 1 Mineral-Fe amendments and aqueous Fe controls utilized in *C. brevispina* coculture experiments to assess the bioavailability of mineral-bound Fe[a]

Exptl treatment	Base M1 medium	Coculture inoculum (%, vol/vol)	Mineral addition		
			Source	Size (μm)	Concn (g liter^{-1})
Fe-depleted (control)	NA-Fe	1[b]	—[c]	—	—
	NA-Fe	—	—	—	—
Fe-EDTA	Fe-EDTA	1	—	—	—
	Fe-EDTA	—	—	—	—
Forsterite [Fo^{90}, $Mg_{1.8}Fe(II)_{0.2}SiO_4$]	NA-Fe	1	San Carlos, NM	75–150	5
	NA-Fe	—	San Carlos, NM	75–150	5
Fe(III) smectite (2:1 phyllosilicate)	NA-Fe	1	Synthetic (64)	38–150	1.5
	NA-Fe	—	Synthetic (64)	38–150	1.5
Pyrite [$Fe(II)S_2$]	NA-Fe	1	Huanzala, Peru	75–150	1
	NA-Fe	—	Huanzala, Peru	75–150	1
Goethite [Fe(III)OOH]	NA-Fe	1	Synthetic (63)	0.1–0.3	0.04
	NA-Fe	—	Synthetic (63)	0.1–0.3	0.04

[a]Parallel noninoculated, abiotic control experiments were conducted for all treatments. Both biotic and abiotic treatments were run in triplicate.
[b]The inoculum was maintained on Fe-EDTA M1.
[c]—, not applicable.

acquisition mechanisms include direct and indirect microbe-mineral interactions such as cell-mineral attachment (27, 28), organic acid production resulting in increased mineral dissolution, and Fe chelation via siderophore production (27, 30, 31). Both types of interactions release nutrients from mineral sources and enhance microbial growth (for examples, see references 25, 27, 29, 32, and 33). Likewise, siderophore-chelated Fe can be utilized by microalgae (23, 24), which in turn produce organic carbon (C_{org}) substrates that support heterotrophic bacterial growth (20, 34). Microalgae may also be capable of mobilizing and using mineral-bound Fe. Algal cell walls host ferric reductase systems (35–37) that may be important in Fe mobility and uptake. Microalgae are known to release extracellular phosphatase and sulfatase under P (38) and SO_4^{2-} (39) limiting conditions, respectively, demonstrating their ability to influence nutrient mobilization.

Here, we utilize *Chloromonas brevispina* (40)-bacterial cocultures to investigate the bioavailability of Fe-bearing minerals as a micronutrient source in supporting snow algal growth in otherwise Fe-depleted systems. Growth in cocultures provided with labile Fe-EDTA and mineral-bound Fe sources was compared to growth under Fe-depleted conditions to investigate the ability of a snow algal-bacterial community to extract and utilize Fe from a range of common Fe-bearing minerals: (i) natural San Carlos forsterite ($Mg_{1.8}Fe_{0.2}SiO_4$, or Fo^{90}) (41), (ii) synthetic Fe(III) smectite (2:1 Fe phyllosilicate), (iii) natural pyrite ($Fe(II)S_2$), and (iv) synthetic goethite (Fe(III)O(OH)). Increased algal cell production and enhanced mineral dissolution in cultures containing Fe-bearing Fo^{90} suggest that mineral-bound elements serve as micronutrient sources for snow algal communities capable of forming albedo-altering blooms.

RESULTS

Experimental design. *C. brevispina*-bacterial coculture growth was monitored under Fe-depleted, Fe-replete (Fe-EDTA), and Fe-bearing mineral conditions to investigate the bioavailability of Fe within mineral dust and its impact on snow algae and coculture growth dynamics. Fe-bearing mineral treatments included the addition of Fo^{90}, Fe(III) smectite, pyrite, or goethite in otherwise Fe-depleted growth medium (Table 1). Mineral dissolution and pH were also monitored over the course of the algal growth cycle to explore the impact of snow microbiota on mineral dust weathering.

Media pH evolution over time. The pH of sterile growth medium used herein was approximately 5.5. All mineral-bearing and Fe-depleted cocultures exhibited an increase in pH over the course of algal growth despite the presence of a phosphate buffer (see Fig. S1 and Tables S1 to S5 in the supplemental material). The largest pH increase was observed in the Fe(III) smectite-bearing cocultures, which exhibited an initial pH of 5.94 (1 day of incubation) in both the abiotic and biotic systems and maximum pHs of 6.18 $\pm$ 0.03 and 6.24 $\pm$ 0.01 (50 days) (Fig. S1), respectively. Biotic pyrite, goethite, and Fe-depleted treatments showed an equivalent increase in pH, up to approximately 5.6. Abiotic pyrite and goethite experiments showed minimal change in pH over the course of the experiments. Fo^{90}-bearing biotic and abiotic experiments underwent a steady increase in pH to 5.90 $\pm$ 0.02 and 5.82 $\pm$ 0.02 (1σ), respectively, after 72 days of incubation, with slightly higher pH values observed in the biotic systems. In contrast, the Fe-EDTA coculture pH decreased from 5.2 to a minimum pH of 4.3 at 27 days of incubation, or the approximate sigmoid midpoint of the algal growth curve (see Fig. 2) (Fig. S1).

Algal growth dynamics. One of the primary factors contributing to the albedo-altering effect of snow algal blooms is total algal biomass (10), which is directly linked to cell density. We therefore used algal cell density (Tables S6 to S10), including cell production rates and coculture-carrying capacity, as a metric to assess the impact of Fe bioavailability on coculture growth across treatments. Algal density during stationary-phase growth for all Fe treatments was determined at 50 days of incubation and compared to algal production in the Fe-depleted condition (Fig. 1). Fe-EDTA-bearing cultures supported the largest algal population ($19.4 \times 10^5 \pm 3.2 \times 10^5$ cells ml^{-1},1σ, time [t] = 50 days) (Fig. 1), which was nearly 4-fold higher ($P = 0.003$) (Table S11) than the stationary-phase algal cell densities in the Fe-depleted growth condition ($5.1 \times 10^5 \pm 0.7 \times 10^5$ cells ml^{-1}, 1σ, $t = 50$ days) (Fig. 1). These data confirm that Fe was a growth-limiting component in the Fe-depleted system in which Fe-EDTA was not added to the medium and that the addition of bioavailable Fe to the Fe-depleted medium, such as in the Fe-EDTA treatment, is capable of stimulating significantly higher algal cell production.

A significant increase in stationary-phase algal cell density was observed in Fo^{90}-bearing treatments ($6.9 \times 10^5 \pm 0.3 \times 10^5$ cells ml^{-1}, 1σ, $t = 50$ days) relative to the Fe-depleted cocultures ($P = 0.02$) (Fig. 1). Algal production was negatively impacted in cocultures containing Fe(III) smectite, which exhibited statistically lower algal cell concentrations after 50 days of incubation ($P = 0.02$) than cocultures in the Fe-depleted condition (Fig. 1). The presence of pyrite and goethite did not result in additional algal or bacterial cell production compared to that of the Fe-depleted cocultures ($P > 0.05$) (Fig. 1). This suggests that pyrite and goethite are unable to promote algal growth in this coculture, possibly due to a combination of their iron oxidation state (Table 1) and mineral stability. Mineral dissolution and cell growth within the pyrite- and goethite-containing treatments were not considered further, since algal growth was not enhanced.

Time-dependent algal cell density data were determined for the Fe-depleted treatment and for the treatments that exhibited significantly higher stationary-phase algal densities than the Fe-depleted condition, namely, the Fo^{90}- and Fe-EDTA-bearing systems (Fig. 2). The Fo^{90}, Fe-EDTA, and Fe-depleted growth conditions exhibited logistical algal growth behavior despite the presence of a bacterial coculture. Exponential algal growth in these three treatments was also temporally associated with a shift in pH, where the pH dropped in the Fe-EDTA treatment and increased in the Fe-depleted and Fo^{90} treatments (Fig. 2; Fig. S1). Best-fit logistic models of the algal growth (Fig. S2 and Table S17) also support the conclusions that the algal carrying capacity of Fo^{90}-bearing systems exceeds that of the Fe-depleted condition. Interestingly, algal doubling times within the Fo^{90} cocultures (5.3 $\pm$ 0.2 days, 2σ) (Fig. S2 and Table S18) were statistically equivalent to those observed in the Fe-EDTA cocultures (5.2 $\pm$ 0.1 days, 2σ) (Fig. S2 and Table S18). In contrast, growth rates within the

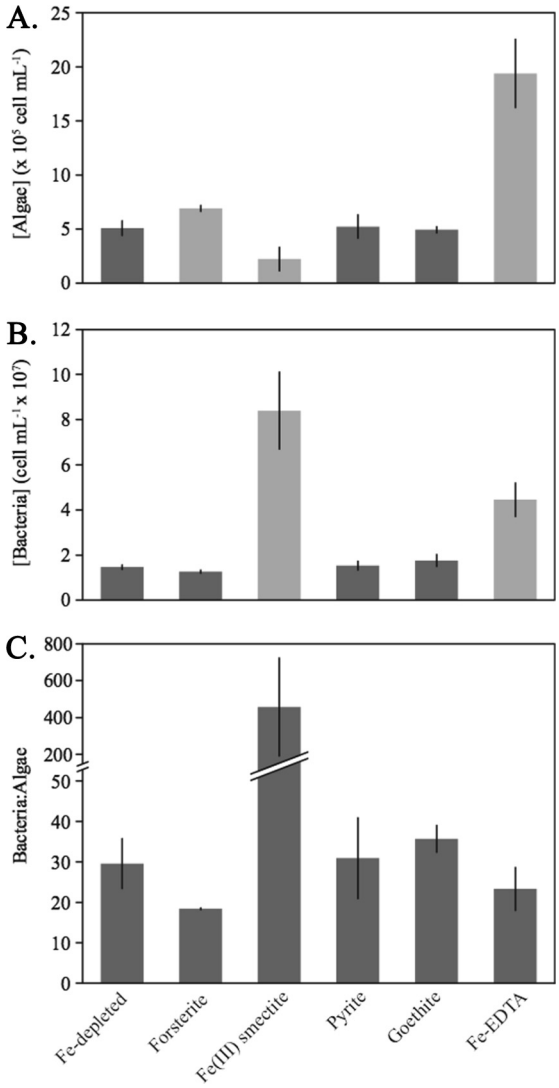

FIG 1 Stationary-phase (t = 50 days of incubation) algal (A) and bacterial (B) cell densities and ratios of bacteria to algae (C) for each Fe treatment. Light gray bars represent significantly different ($P < 0.05$) results relative to growth in the Fe-depleted control.

Fe-depleted cocultures exhibited a significantly longer doubling time (8.1 ± 0.5 days, 2σ) (Fig. S2 and Table S18). Fo^{90}-bearing cocultures also reached stationary-phase growth more rapidly than the Fe-depleted and Fe-EDTA-containing cocultures, as reflected by the sigmoid midpoints (t_{half}) at 21.8 ± 1.0, 29.5 ± 0.7, and 28.7 ± 2.2 days of incubation, respectively (Table S17).

Bacterial growth and ratios of bacteria to algae. After 50 days of incubation (Tables S12 and S13), Fe-depleted cocultures had approximately 30 times more bacterial cells than algal cells (Fig. 1) and the ratios of bacteria to algae were statistically similar to the ratios observed for the pyrite- and goethite-bearing cocultures. Slightly lower ratios of bacteria to algae (~20:1) were measured in the Fo^{90}- and Fe-EDTA-bearing systems at 50 days of incubation (Fig. 1) than in the Fe-depleted growth condition ($P > 0.05$) (Table S11).

The largest deviation in the ratio of bacteria to algal cells was observed in the Fe(III) smectite-bearing cocultures, where the average ratio across triplicates was 457 ± 270 after 50 days of incubation ($P = 0.11$) (Fig. 1 and Table S11). We conclude that the Fe(III) smectite-bearing cocultures exhibited a different community structure, based on both the significantly higher bacterial densities ($P = 0.02$) and lower algal cell densities ($P = 0.02$) than of the Fe-depleted condition (Fig. 1).

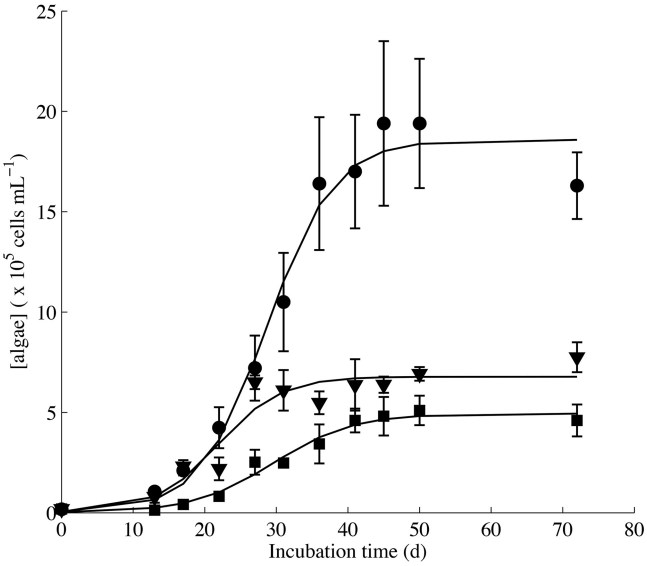

FIG 2 Snow algal growth in the Fe-depleted (control, squares)-, Fe-EDTA (circles)-, and Fo^{90} (triangles)-bearing experimental cocultures exhibit logistical growth dynamics as modeled by the best-fit logistical growth curves (black lines). Algal concentrations for Fo^{90} and Fe-EDTA systems exhibit a carrying capacity above that of the Fe-depleted control cocultures. Algae in Fe-EDTA systems appeared to enter death phase after 72 days of incubation, while algal concentrations in Fo^{90}-bearing cultures were stable or slightly increased at the end of the experiment. Error bars are 1σ standard deviation of triplicates.

Bacterial cell densities determined over the duration of incubation for the Fe-depleted and Fo^{90}- and Fe-EDTA-bearing cocultures (Tables S14 to S16) generally increased over time but did not exhibit a clear logistical growth pattern or achieve a stationary growth phase (Fig. S3). Fe-depleted cocultures initially exhibited an exponential growth pattern, but bacterial cell concentrations dropped and subsequently recovered between 20 and 30 days of incubation. This trend was reflected in the Fo^{90}-bearing cultures to a lesser degree and nearly disappeared in the Fe-EDTA cultures (Fig. S3).

Interestingly, the ratios of bacteria to algae for each of these systems achieved a steady state that coincides with exponential to early stationary algal growth phases (Fig. S4). We averaged the ratios of bacteria to algae from the respective algal growth sigmoid midpoints to early stationary-phase growth, corresponding to 45 days of incubation. Steady-state ratios of bacteria to algae for the Fe-depleted, Fo^{90}, and Fe-EDTA systems were 27.9 $\pm$ 7.4, 19.2 $\pm$ 3.9, and 22.2 $\pm$ 6.5 (1σ), respectively. The steady-state ratio of bacteria to algae in the Fo^{90}-bearing system was statistically lower ($P = 0.01$) than that of the Fe-depleted condition. An increase in the ratio of bacteria to algal cells was observed in both the Fe-EDTA and Fe-depleted systems at the 72-day incubation time point but not in the Fo^{90}-bearing system, further suggesting the impact of Fo^{90} on algal growth dynamics.

Coculture bacterial diversity. Cocultures originating from the B SNO96 *C. brevispina* strain contained abundant bacterial cells (Fig. 1). A total of 107 bacterial operational taxonomic units (OTUs) (excluding singletons), and no archaea, were identified within the Fe-EDTA M1-maintained *C. brevispina* coculture. Eight OTUs comprised 99% of the total 16S rRNA gene sequences (Fig. 3). Of these eight OTUs, seven families were present, including *Pseudomonadaceae* (41.0%), *Xanthomonadaceae* (21.5%), *Comamonadaceae* (15.6%), *Oxalobacteraceae* (11.1%), *Sphingobacteriaceae* (6.5%), *Enterobacteriaceae* (1.7%), and *Burkholderiaceae* (1.6%). Six of the top eight OTUs were discernible to the genus level and included *Pseudomonas* (41.0%), *Variovorax* (15.6%), *Pedobacter* (6.5%), *Collimonas* (11.1%), *Rhodanobacter* (7.7%), and *Burkholderia-Paraburkholderia* (1.6%). Cultivation efforts on M1 medium without iron (NA-Fe M1) containing uncharacterized *C. brevispina* photosynthates as the carbon source (M1P)

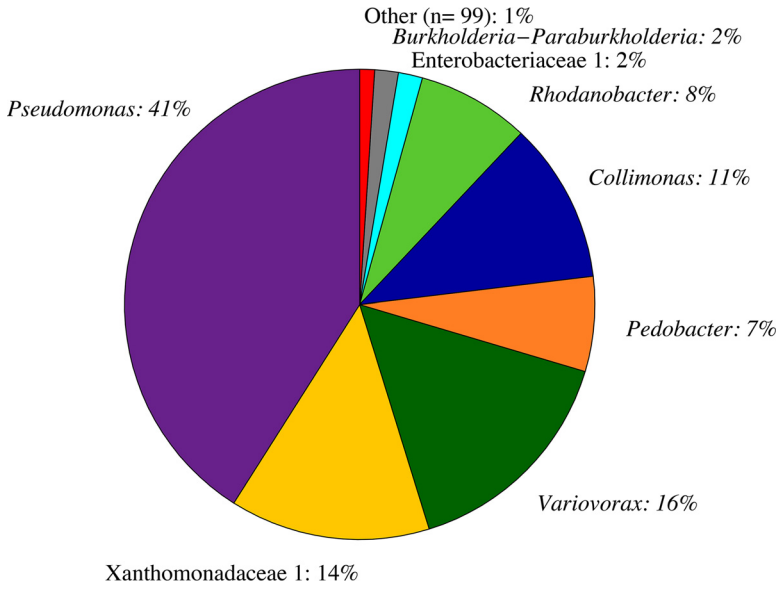

FIG 3 Taxonomic distribution of 16S rRNA gene-derived OTUs from an exponential-phase *C. brevispina*-bacterial coculture grown on Fe-replete (Fe-EDTA) M1 medium (percentages sum to 102% due to rounding). OTUs are labeled based on the highest-confidence, discernible taxonomical level.

yielded three *Pedobacter* isolates that were not different over 500 bases of the 16S rRNA gene.

Mineral dissolution. Mineral dissolution was investigated via changes in Si, Mg, and Fe concentrations (Tables S19 to S23) over time for cocultures that exhibited significant differences in algal or bacterial growth relative to the Fe-depleted condition, namely, the Fo^{90}- and Fe(III) smectite-bearing biotic and abiotic systems. Aqueous Fe concentrations in the Fe-depleted and Fo^{90} and Fe(III) smectite treatments, for both the biotic and abiotic systems, were typically in the submicromolar range (<0.8 μM) and did not exhibit a trend over the duration of the experiments. Mean aqueous Fe concentrations for all time points in the abiotic and biotic Fo^{90}-bearing, Fe(III) smectite, and Fe-depleted systems were 0.40 $\pm$ 0.42 μM (1σ), 0.57 $\pm$ 0.48 μM (1σ), and 0.16 $\pm$ 0.18 μM (1σ), respectively.

Mg concentrations within Fe-depleted cocultures decreased linearly over time (-0.27 μM day^{-1}, $R^2 = 0.95$) (Fig. S5), suggesting biotic Mg uptake. Si concentrations in the Fe-depleted condition exhibited no trend over the duration of the experiments (Fig. S5), indicating that aqueous Si was conservative and was not impacted by microbial growth or uptake. We therefore examined Fo^{90} and Fe(III) smectite dissolution based on Si release.

Si release due to Fo^{90} dissolution in both the biotic and abiotic systems generally exhibited a linear increase over time (Fig. 4) and is described with best-fit linear models (0 to 72 days, $R^2 = 0.96$). Si concentrations were slightly higher in the biotic Fo^{90} system, and best-fit linear models yielded a higher, biotically enhanced Fo^{90} dissolution rate (log $r_{Fo90,\ Si} = -10.23 \pm 0.03$ mol m^{-2} s^{-1}, 95% confidence interval [CI]) relative to that of abiotic Fo^{90} dissolution (log $r_{Fo90,\ Si} = -10.30 \pm 0.03$ mol m^{-2} s^{-1}, 95% CI). An initial more-rapid release of Si (0 to 13 days) was also observed in the biotic Fo^{90} systems (Fig. 4).

Initial Mg release (0 to 13 days) in the biotic, Fo^{90}-bearing system was also more rapid than abiotic Mg release (Fig. S6). After 13 days of incubation, however, the effect of microbial uptake became apparent within the biotic cultures in the form of a pronounced drop in Mg accumulation and a deviation from linear Mg release (Fig. S6). Stoichiometric dissolution in the abiotic Fo^{90} dissolution systems is achieved after approximately 30 days, whereas Mg/Si ratios in the biotic systems are below stoichiometric ratios (Fig. 5).

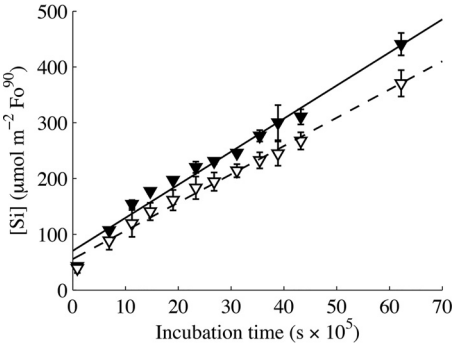

FIG 4 Si concentration as a function of time in biotic (closed triangles) and abiotic (open triangles) forsterite dissolution systems over the duration of incubation. Best-fit linear models for both biotic (solid line) and abiotic (dashed line) forsterite dissolution rates have a 0.92 R^2 fit.

Fe(III) smectite dissolution exhibited higher than expected Si concentrations (>900 μM, t = 72 days), a nonlinear Si release profile over the duration of incubation (Fig. S7), and a large increase in pH (6.20 ± 0.02, 22 days) (Fig. S1). The dissolution behaviors in the biotic and abiotic, Fe(III) smectite-bearing systems are equivalent despite bacterial biomass production in the biotic systems.

DISCUSSION

Forsterite as an Fe source for snow algae. Fe limitation can negatively impact algal growth in numerous ways, including, but not limited to, diminished chlorophyll production (i.e., chlorosis), inefficient energy production, and decreased cell densities (16). Of these Fe limitation symptoms, algal cell densities and total biomass are likely the largest factors determining the albedo-altering potential of snow algal blooms (10). We therefore focused on algal cell density in examining the potential for Fe-bearing minerals to support snow algal blooms.

C. brevispina snow algae in coculture with bacteria exhibited higher cell densities in the presence of Fo^{90} than in the Fe-depleted cocultures (Fig. 1 and 2). It is important to note that an overall pH increase from 5.5 to 5.9 was observed in the abiotic and biotic Fo^{90}-bearing conditions. This pH increase is expected due to proton (H^+) uptake via an acidic, silicate dissolution mechanism (42). It is also possible that the pH increase in mineral-containing and Fe-depleted biotic systems was due in part to a bottle effect in which algal growth may have lowered the partial pressure of CO_2, although it should be noted that the pH decreased in the Fe-EDTA system. CO_2 uptake by snow algae and a subsequent increase in pH was also observed by Hoham (43) at field sites in New York and Quebec. Acidophilic *Chloromonas* snow algae exhibit optimal growth between pH

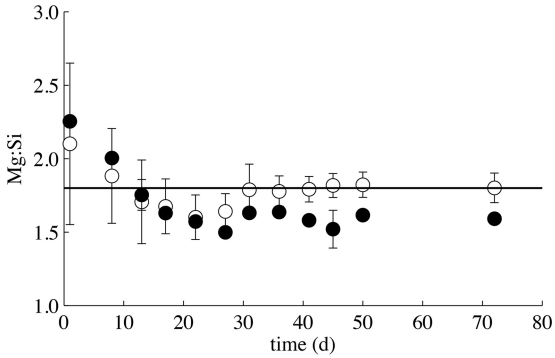

FIG 5 Mg/Si ratio for biotic (closed circles) and abiotic (open circles) Fo^{90} dissolution systems over the duration of incubation. Abiotic dissolution systems achieve stoichiometric dissolution (black line) after approximately 30 days of incubation. The stoichiometry of Fo^{90} dissolution in biotic systems falls below the stoichiometric ratio due to Mg uptake by algal and bacterial growth.

4 and 5 (44). Even a pH increase of 0.5 (e.g., from pH 5.5 to 6.0) has been shown to negatively impact *Chloromonas* sp. concentrations (44). It is possible that the Fo^{90}-bearing systems could support even higher algal growth in the absence of a pH increase. The importance of this pH effect is further corroborated by significantly lower algal cell densities in the Fe(III) smectite-bearing cocultures (Fig. 1) than in the Fe-limited cocultures, where the pH rose to 6.2 after 22 days of incubation.

Even though cocultures were provided with a mineral-bound rather than aqueous Fe source, algal doubling times within the Fo^{90}-containing treatments (5.3 $\pm$ 0.2 days, 2σ) were equivalent to those observed in the Fe-EDTA treatments (5.2 $\pm$ 0.1 days, 2σ), while they were significantly lower than algal doubling times in the Fe-depleted cocultures (8.1 $\pm$ 0.5 days, 2σ). The snow algal growth rates in the Fo^{90}-bearing treatments suggest that Fo^{90} provides, at least initially, a sufficient amount of Fe to support growth rates similar to those observed in Fe-replete conditions. This also indicates that the Fe within Fo^{90}, or the dissolution products of Fo^{90}, is bioavailable to the coculture and ultimately to *C. brevispina*.

Although the initial algal growth rate of the Fo^{90}-bearing cocultures was relatively high, it was rapidly tempered with stationary-phase growth occurring after approximately 27 days, compared to the growth in the Fe-depleted and Fe-EDTA-bearing systems, which reached stationary phase around 45 to 50 days (Fig. 2). Algae in the Fe-depleted and Fe-EDTA systems also exhibited a drop in cell concentrations at 72 days of incubation (Fig. 2), at which time the ratio of bacteria to algae also increased (see Fig. S4 in the supplemental material). These data suggest a transition into algal death phase and an increase in bioavailable C_{org}, possibly due to algal cell lysis. In the Fo^{90}-bearing cocultures, however, algal cell densities remained steady, or even increased slightly (Fig. 2), at 72 days of incubation, and the steady-state ratio of bacteria to algae was maintained (Fig. S4). These results may be indicative of long-term Fo^{90} Fe bioavailability affecting algal cell health over time.

These increases in the snow algal carrying capacity and growth rate in the Fo^{90}-bearing cocultures (Fig. 2; Table S18) suggest that Fe-mineral dust, especially olivine mineral dust, in snow is capable of supporting increased algal cell densities relative to "clean," low-dust snow and may be an important factor in stimulating the formation of albedo-altering snow algal blooms. It is interesting to note that the regional geology at the snow algal coculture source (Lac Laflamme, Quebec, Canada), known as the Grenville formation, is characterized by felsic to mafic metamorphic and igneous formations (45). The mineralogy of these rock types includes olivine and other iron-bearing silicic minerals (45). It is possible that the *C. brevispina*-bacterial coculture is adapted to extracting Fe from silicic mineral dust similar to the iron-bearing Fo^{90} used in this work.

Ratio of bacteria to algae and bacterial community. Fe availability impacts microbial community structure in marine environments, including relative densities of microalgae and bacteria (16). Ratios of bacteria to algae in the Fo^{90}- and Fe-EDTA-bearing systems at 50 days of incubation were slightly lower than those determined for the Fe-depleted system (Fig. 1) and were significantly ($P = 0.01$) lower in the Fo^{90} treatments (19.2 $\pm$ 3.9, 1σ) relative to the Fe-depleted cocultures (27.9 $\pm$ 7.4, 1σ) when taking into account steady-state ratios of bacteria to algae measured over the course of coculture incubation (Fig. S4). It is possible that bioavailable mineral-bound Fe in an otherwise Fe-depleted system has a larger impact on the concentration of snow algae than on associated bacteria due to the relatively higher Fe requirements of photosynthetic organisms than of heterotrophic bacteria (16). Higher algal/bacterial C ratios have also been observed in red snow than in white snow in the Sierra Nevada, California (34), and in Fe-amended waters than in natural marine waters (17).

Numerous studies have identified partnerships between bacteria and algae (for examples, see references 22 to 24). Amin et al. (24) and Keshtacher-Liebso et al. (23), in particular, identified bacterial-algal partnerships where bacteria increased the bioavailability of Fe via siderophore complexation and subsequent photolysis, while algae

provided C_{org} that supported heterotrophic bacterial growth. Three aspects of algal and bacterial growth dynamics observed herein suggest bacterial-algal partnerships within the cocultures: (i) algal populations within the Fe-EDTA, Fe-depleted, and Fo^{90} treatments exhibited typical logistic growth patterns (Fig. 2), while the bacterial populations did not (Fig. S3); (ii) ratios of bacteria to algae measured during exponential and early stationary-phase algal growth (Fig. S4) were relatively constant, suggesting that the algal populations may have controlled the growth of bacteria by supplying C_{org}; and (iii) the increase in the ratio of bacteria to algae in the Fe-EDTA and Fe-depleted cultures after 72 days of incubation, coupled with the initiation of the algal death phase, suggests a shift in the microbial community, where algal cell lysis supported an increase in the heterotrophic bacterial population. Bacterial growth on NA-Fe M1 agar plates containing photosynthates as the only C_{org} source further suggests that the bacteria within the cocultures, and in particular the *Pedobacter* isolates, are capable of utilizing photosynthates as their carbon source. It is also notable that the Fo^{90} system exhibited stable ratios of bacteria to algae (Fig. S4) as well as stable to slightly increasing algal concentrations out to 72 days of incubation (Fig. 2). These data suggest that mineral iron sources may stabilize snow algal communities and extend the duration of snow algal blooms or may negatively impact bacterial populations.

The 16S rRNA gene-derived bacterial OTUs ($n = 107$, excluding singletons) within the Fe-EDTA coculture represent the inoculum introduced into each of the snow algal-bacterial coculture treatments described herein (Fig. 3). This bacterial community likely reflects both the pressures of laboratory culturing conditions and the origin of the field sample, i.e., Lac Laflamme, Quebec, Canada. It is additionally possible that the bacterial community in each Fe treatment shifted relative to the inoculum community due to the imposed Fe-depleted conditions and available Fe-mineral sources.

However, a generalized assessment of bacterial taxonomy and environmental occurrence suggests that the microbiota detected resemble natural communities associated with snow algae. Lutz et al. (3, 46) generally noted *Bacteroidetes* and *Proteobacteria* as major phyla found with red snow algal blooms collected in the Arctic. These same phyla comprise >99% of the bacteria in the coculture studied herein. Members of the bacterial classes *Gammaproteobacteria*, *Betaproteobacteria*, and *Sphingobacteria* comprise the top eight OTUs (>1%) within the *C. brevispina* coculture and are commonly found in snow and ice environments (12, 47–49). Bacterial communities associated with red snow algae in the Arctic generally contained members of *Betaproteobacteria* and *Sphingobacteria* (46), classes that comprise 28.3% and 6.5% of 16S rRNA gene sequences, respectively, in the *C. brevispina* cocultures. *Betaproteobacteria*, in particular, were also found to dominate green snow algal blooms in the Arctic (46). The *Sphingobacteria* genus *Pedobacter*, which comprises 6.5% of the 16S rRNA gene sequences in the *C. brevispina* coculture, has been identified in red snow containing *Chlamydomonas nivalis* (50) and glacier snow (51).

Pseudomonas and *Collimonas* species, identified within the coculture, are known to enhance mineral weathering processes, including increasing Fe solubility and release from Fe-bearing silicate minerals (32, 52, 53). Species in the genus *Pseudomonas*, the dominant OTU (41.0%) in the *C. brevispina* cocultures, include common soil bacteria capable of producing siderophores (54–56). Low (i.e., micromolar) iron concentrations have also been shown to trigger large shifts in *Pseudomonas* sp. gene expression (57), increased biofilm formation (56, 58, 59), and siderophore production (54, 56).

The *C. brevispina* coculture also contained an OTU identified as a *Collimonas* sp. (11.1%). Members of the *Collimonas* genus are typically associated with slightly acidic oligotrophic soil environments (52). Members of this genus have also been isolated from tundra soil and successfully grown at 0°C (60). *Collimonas* species are known to mobilize Fe from Fe-bearing minerals such as biotite via culture acidification and the production of siderophores (32, 52). It is possible that these and other bacteria within the *C. brevispina* cocultures play a role in mobilizing Fe from Fo^{90} or its dissolution products and in increasing Fe bioavailability to *C. brevispina*.

Biologically enhanced forsterite dissolution and mineral bioavailability. Fo^{90} dissolution in acidic solutions proceeds via hydrogen ion exchange with Mg and Fe(II) to form a Si-rich, cation-leached layer on the mineral surface (42, 61). The occurrence of this cation-leaching dissolution mechanism in our experiments is corroborated by high initial Mg/Si ratios in solution that exceed the stoichiometric ratio of Fo^{90} in both the biotic and abiotic dissolution systems (Fig. 5). Stoichiometric dissolution is achieved after approximately 30 days in the abiotic Fo^{90} dissolution systems (Fig. 5). In contrast, Mg/Si ratios are below stoichiometric values in the biotic systems, suggesting Mg uptake. Based on stoichiometric Mg/Si dissolution in abiotic systems, and using the Si concentration as a metric for total Fo^{90} dissolution, total Fe release would have reached 39.6 μM and 48.0 μM after 72 days of incubation for abiotic and biotic dissolution systems, respectively. Low aqueous Fe concentrations (0.32 $\pm$ 0.37 μM, 1σ) were measured in the abiotic and biotic Fo^{90}-bearing, as well as Fe-depleted, systems. These low aqueous iron concentrations are expected, since Fe(II) released during dissolution likely undergoes rapid oxidation to Fe(III) and precipitates as an Fe oxide in the aerobic, near-neutral cultures.

Mineral-bound Fe, in this case either within Fo^{90} or as a secondary Fe(III) precipitate, is accessible to the coculture and microbial life in general through direct or indirect microbe-mineral interactions. These interactions include, but are not limited to, microbe-mineral contact, the production and release of organic acids, and element chelation via exudates such as siderophores (for examples, see references 27 to 29, 33, and 62). Both abiotic and microbially mediated cation surface leaching are expected to deplete the amount of iron exposed at the Fo^{90} mineral surface under these acidic to circumneutral pH conditions. This surface leaching also inhibits access to fresh mineral-Fe reserves as a Si-rich layer forms (61). This dissolution model fits with the observed rapid algal growth rate when Fo^{90} mineral surfaces are fresh and provide abundant iron, followed by stationary growth once bioavailable iron exposed at the mineral surface has likely been depleted and biologically assimilated (Fig. 2). As mineral dissolution proceeds, and despite the presence of leached layers, slow continued release of Fe appears sufficient to support algal maintenance metabolism and the stationary-phase algal population in Fo^{90} cultures out to 72 days of incubation (Fig. 2).

Fe(III) smectite and preferential bacterial growth. Fe(III) smectite-bearing treatments exhibited anomalous behaviors in terms of their mineral dissolution, pH, and biologic growth compared to all other systems. The initial high rate and curvilinear dissolution of Fe(III) smectite over time suggest the presence of a highly reactive silica component that is not representative of the smectite. We therefore abstained from quantifying a Fe(III) smectite dissolution rate. Despite high bacterial growth, silica release in the biotic systems was equivalent to that of the abiotic Fe(III) smectite bearing systems (Fig. S7), suggesting that dissolution was dominated by abiotic processes. Abiotic dissolution of this highly reactive silica component likely resulted in the pH increase in both the biotic and abiotic Fe(III) smectite-bearing systems (Fig. S1). The relatively low algal levels in the Fe(III) smectite-bearing cocultures (Fig. 1) are likely due to the observed pH increase (Fig. S1). Algal cell lysis, and the release of C_{org} from algae, associated with the pH increase, may be responsible for the higher bacterial populations and ratios of bacteria to algae. It is possible, however, that the microbial community utilized iron provided by the Fe(III) smectite.

Conclusion. Mineral-bound Fe within Fo^{90}, and/or its dissolution products, was bioavailable to a *C. brevispina* snow algal-bacterial coculture as evidenced by (i) an increase in snow algal levels in Fo^{90}-bearing systems relative to the Fe-depleted treatment, (ii) an algal growth rate in Fo^{90} cocultures equivalent to those in Fe-replete cocultures and that was significantly higher than rates in the Fe-depleted control, and (iii) microbially enhanced Fo^{90} dissolution. These data provide unequivocal evidence that mineral dust can support elevated snow algal growth in otherwise Fe-depleted systems. Extrapolation to natural systems suggests that the presence of Fe-bearing silicate minerals, olivine in particular, in snow and associated with algal surfaces may play an important role in stimulating and supporting albedo-altering snow algal blooms.

To date, the majority of studies have found few to no correlations between Fe concentrations and snow algal blooms (3, 12). However, qualitative observations of field samples show that mineral dust was directly associated with *Chlamydomonas* snow algal cell surfaces (13, 14), which may provide micronutrients required for growth. It is possible that these findings can be explained at least in part by the mineral-bound Fe bioavailability, Fe(III) insolubility, and biological Fe uptake and assimilation discussed here. More work is required to elucidate the influence of Fe-bearing mineral dust, mineralogy, and the role of microbial partnerships in stimulating and supporting natural snow algal blooms.

MATERIALS AND METHODS

Mineral synthesis and preparation. The ability of a snow algal-bacterial coculture to extract and utilize mineral-bound Fe was tested using four Fe-bearing mineral powders: (i) natural San Carlos Fo^{90} (41), (ii) synthetic Fe(III) smectite, (iii) natural pyrite, and (iv) synthetic goethite. Goethite and Fe(III) smectite were synthesized as described below to produce high-purity mineral substrate.

Goethite was synthesized under alkaline conditions (63). Briefly, 90 ml of 5 M KOH was mixed with 50 ml of 1 M $Fe(NO_3)_3 \cdot 9H_2O$ and diluted to 1 liter in an acid-washed polyethylene or polypropylene bottle. The resultant red-brown ferrihydrite was incubated at 70°C for 60 h to produce synthetic, orange-yellow goethite (63). The final goethite product was separated into 50-ml aliquots and pelleted via centrifugation at 1,500 relative centrifugal force (rcf) for 5 min, the supernatant was decanted, and the pellet was resuspended in 50 ml of 18 MΩ cm^{-1} H_2O. This washing process was repeated 6 times to remove residual OH^- and NO_3^- anions, until the pH of the rinsate was 7.6. The mineral product was subsequently lyophilized to remove residual rinsate. Synthetic goethite forms needle-like, acicular crystals approximately 0.1 to 0.3 μm in length (63) and was used without additional crushing or sieving.

Fe(III) smectite, a 2:1 Fe phyllosilicate, was synthesized as described by Mizutani et al. (64). Briefly, Fe(III) smectite synthesis was achieved by acidifying 420 ml of 45 mM Na_2SiO_3 to pH 3 with the addition of 43.5 ml of 0.5 M H_2SO_4 and subsequently adding 4.2 g $Na_2S_2O_4$ and 3.94 g of $FeSO_4 \cdot 7H_2O$. Precipitate was formed by the addition of 19.8 ml of 5 M NaOH and allowed to mature for 24 h at room temperature (20°C). The precipitate was resuspended, transferred to Teflon-lined Parr pressure vessels, and treated at 150°C for 48 h. Following heat treatment, the supernatant was decanted and the final product was pelleted via centrifugation in 50-ml centrifuge tubes at 6,678 rcf for 5 min and washed by sequentially decanting the supernatant and resuspending the pellet in 18 MΩ cm^{-1} H_2O, for a total of five wash cycles. Finally, the synthetic Fe(III) smectite was air dried at room temperature and prepared for dissolution experiments as described below.

San Carlos Fo^{90} (VWR Scientific) is a 10% Fe-substituted, Mg-rich end member of the olivine solid solution series chosen for its purity (41). Naturally occurring pyrite was acquired from Wards Science. Fo^{90}, pyrite, and Fe(III) smectite were crushed with an agate mortar and pestle and sieved. Sieve fractions from 75 to 150 μm were utilized in Fo^{90} and pyrite dissolution experiments, while 38- to 150-μm sieve fractions were used in the Fe(III) smectite dissolution experiments.

We refrained from autoclaving the mineral powders in order to prevent mineral alteration and oxidation known to occur under the hot and humid autoclaving conditions (for examples, see references 65 and 66). Crushed and sieved pyrite was immersed in 100 ml of 1 N HCl for 7 h to remove oxidized iron from the surface. Removal of adsorbed fines and mineral sterilization, for all mineral powders, was achieved by suspension and sonication in ethanol, with the supernatant decanted following each of three sonication steps lasting 3 min, 1 min, and 30 s. Finally, the mineral powders were gently resuspended in ethanol and dried at room temperature. Mineral powder surface areas were determined only for those minerals which resulted in increased algal growth, namely, the Fo^{90}-bearing system. We calculated a specific surface area of 0.118 m^2 g^{-1} for the 75- to 150-μm Fo^{90} (see Table S24 in the supplemental material) (67).

Snow algal coculture-mineral experimental design. The ability of snow algal communities to utilize mineral-bound Fe as a trace nutrient source was tested using a *C. brevispina*-bacterial coculture. Cocultures were provided by James Raymond and purchased from the Culture Collection of Algae, University of Texas, Austin (UTEX B SNO96). The *C. brevispina* coculture was originally collected and isolated by Ronald Hoham, from Lac Laflamme, Quebec, Canada. *C. brevispina* cocultures were maintained on M1 growth medium, also referred to as Fe-EDTA growth medium, as described by Hoham et al. (40). Briefly, M1 growth medium (40) was prepared in acid-washed flasks and autoclave sterilized prior to the addition of vitamins and inoculation. Vitamin solutions of 5 mg ml^{-1} biotin and 1 mg ml^{-1} vitamin B_{12} and thiamine-HCl were filter sterilized (0.2-μm pore size) and added aseptically to autoclaved M1 growth medium for a final concentration of 0.1% (vol/vol) each (40). NA-Fe M1 medium for use in biotic and abiotic Fe-bearing mineral experiments and the Fe-depleted treatment was prepared as described above but with the omission of Fe-EDTA and the addition of a trace metal solution without Fe. Both Fe-EDTA M1 and the NA-Fe M1 culture media had an initial pH of ~5.4.

Mineral powders, prepared as described above, were added to NA-Fe M1 medium as the predominant Fe source (Table 1; Table S25). The mass of powder added for each mineral treatment was selected based on Fe content, powder size fraction, dissolution rate, and potential for pH change as dissolution proceeded. Biotic controls included *C. brevispina* coculture growth on Fe-EDTA and NA-Fe M1 growth media. All biotic conditions were inoculated with 1% (vol/vol) *C. brevispina* coculture maintained on Fe-EDTA growth medium, for an initial algal cell concentration of $1.81 \times 10^4 \pm 0.07 \times 10^4$ cells ml^{-1}. A

C. brevispina coculture with high biomass, coupled with a small inoculum volume (1%), was chosen as the inoculum to minimize Fe-EDTA carryover. Maximum Fe-EDTA carryover from a 1% (vol/vol) inoculum is 4.5 μM Fe-EDTA, which assumes that no Fe uptake occurred in the inoculum coculture during growth, although Fe uptake undoubtedly occurred. These low concentrations and observed decreased algal growth in inoculated, NA-Fe M1 medium mean that the growth conditions described as Fe-depleted in the manuscript are also Fe limiting. Parallel abiotic mineral dissolution controls were prepared in the NA-Fe M1 medium. All biotic conditions and abiotic controls were prepared in triplicate (Table S25).

All cultures (170-ml initial volume) were prepared in 250-ml TriForest polycarbonate, baffled-base Erlenmeyer culture flasks acid washed in 10% nitric acid and triple rinsed with 18.2 MΩ cm^{-1} H_2O. Culture flasks were sealed with TriForest DuoCAPs and mixed twice per day for 30 min, once each during the illumination and dark cycles. Three SunBlaster, T5 high output fluorescent grow lamps provided cultures with 2,700 $\pm$ 470 lux on a 16-h-light/8-h-dark cycle. Lux output from the lamps decreased over time to 2,170 $\pm$ 500 lux after 72 days of incubation. Cultures were incubated at 4.0 $\pm$ 0.1°C.

All experiments were sampled aseptically every 4 to 5 days for 50 days of incubation and once at the end of the 72-day incubation. Cultures were vortexed and hand swirled immediately prior to sample removal to resuspend algae and mineral fractions to maintain the microbe-to-mineral ratio over time. Samples were collected for algal and bacterial cell counts, aqueous geochemical analyses, and pH. Cell count samples were fixed with 1.9% filter-sterilized formaldehyde immediately after sample collection and stored at 4°C prior to enumeration. Samples collected for aqueous geochemical analyses were filtered through a 0.2-μm nylon filter to remove cells and mineral. Sample pH was measured on a separate aliquot at the time of sampling on a Mettler Toledo InLab Expert Pro pH probe calibrated with 3 NIST standards. Initial coculture pH was measured on combined samples from triplicate experimental bottles and do not include errors. Later measurements were collected on each individual triplicate and include 1σ errors.

Cell density determination. Total algal biomass, which is directly correlated with algal cell density, is a major factor determining the albedo-altering effect of snow algal blooms. We therefore used algal cell density, cell production rates, and coculture carrying capacity as metrics for Fe bioavailability in each coculture condition. Algal growth for each biotic treatment was determined via direct cell counts. Formaldehyde-fixed samples were resuspended by vortexing, and 10-μl aliquots were loaded into disposable hemacytometer chambers (Incyto C-Chip; Neubauer Improved). Algal cells were counted at $\times$100 magnification (Olympus BH microscope). For samples with low to moderate algal cell densities (1×10^4 to 1×10^6 cells ml^{-1}), cells were counted within each of four to nine large grid zones. Samples with high cell densities ($>1 \times 10^6$ cells ml^{-1}) were counted in 9 to 13 small central grid zones. Algal cell density was determined based on the manufacturer's instructions (Incyto C-Chip; Neubauer Improved). Cell densities for each biotic system were enumerated at 50 days of incubation, or stationary growth phase, to provide an initial comparison across all treatments. Algal cell densities for all time points were enumerated for the Fe-depleted cocultures and those treatments which exhibited stationary-phase growth above the Fe-depleted coculture, namely, the Fo^{90}- and Fe-EDTA-containing systems (Fig. 2).

Bacterial densities were determined based on direct counts from 10 randomly chosen fields of view at $\times$1,000 magnification via epifluorescence microscopy enumeration as described by Porter and Feig (68). Briefly, formaldehyde-fixed samples were vortexed and diluted to between 1 and 25% (vol/vol), up to 1-ml total volume, in filter-sterilized 18 MΩ cm^{-1} H_2O. Diluted samples were stained by adding 0.1% (vol/vol) concentrated DAPI (4′,6-diamidino-2-phenylindole) and incubated in the dark for 15 min prior to resuspending and filtering the sample onto 0.2-μm black polycarbonate filters (Whatman, Nuclepore). Cells were enumerated in 10 random 100-μm fields on a Zeiss Axio Imager microscope equipped with a Hamamatsu ORCA Flash 4.0 LT monochromatic digital CMOS camera. Algal and bacterial cell densities and ratios were compared between Fe-bearing systems and the Fe-depleted treatment using a two-tailed unpaired *t* test based on either equal or unequal variance as determined via the F-test (Table S11).

Aqueous geochemical analyses. Samples collected for elemental concentration analyses were gravimetrically diluted with matrix-matched Fe-, Si-, and Mg-free M1 medium up to 10 times in acid-washed, 15-ml Falcon tubes and acidified to 1% (vol/vol) with concentrated, trace metal-free HNO_3 (OmniTrace nitric acid; VWR). Si, Mg, and Fe concentrations were analyzed on a Thermo Fisher iCAP Q inductively coupled plasma mass spectrometer (ICP-MS) equipped with an automated sampler (see supplemental data). Si and combined Mg and Fe standards were prepared from 1,000-ppm ICP stock solutions (Si, RICCA Mg, Aristar PLUS; Fe, RICCA). Maximum and minimum standard concentrations bracket the concentrations of samples analyzed. Linear standard calibration curves fit to analyte (^{24}Mg, ^{28}Si, and ^{57}Fe) concentration versus counts per second (cps) for 5 to 7 standards yielded R^2 values of 0.999 or better (Fig. S8). Quality control measures resulted in less than $\pm$10% error over the course of ICP-MS analysis.

Modeling cell growth and mineral dissolution. Triplicate snow algal concentration data spanning 0 to 72 days ($n = 33$) of incubation were modeled using the logistical growth equation (equation 1):

$$C_{\text{algae}}(t) = \frac{C_{\text{algae,max}}}{1 + e^{-r(t - t_{\text{half}})}} \quad (1)$$

where C_{algae} (t) is the concentration of snow algae at time t, model-derived $C_{\text{algae, max}}$ is the maximum concentration of algae or carrying capacity of the coculture, t_{half} is the time at the sigmoid midpoint, and r is the slope at the sigmoid midpoint. Best-fit logistic curve parameters were optimized in MATLAB (Table S17).

Exponential growth rate models (equation 2) were fit to triplicate algal concentration data from 0 days of incubation up to one time point beyond the best-fit t_{half} value determined from the logistic

growth models (Table S17). These data include 0 to 27 days of incubation for Fo^{90}-bearing cultures ($t_{half} \approx 22$ days) and 0 to 31 days of incubation for the Fe-EDTA and Fe-depleted cocultures ($t_{half} \approx 30$ days) (Table S18; Fig. S2):

$$C_{algae}(t) = C_{algae,0}\ e^{rt} \quad (2)$$

where C_{algae} (t) is the concentration of algae at time t. The initial algal concentration in the experiment resulting from inoculation before growth has occurred ($C_{algae,0}$ $t = 0$ days) is input as a fixed parameter, and the best-fit exponential rate (r) is solved (Table S18) using nonlinear least-squares curve fitting in MATLAB. The goodness of fit (R^2) for Fe-depleted, Fe-EDTA, and Fo^{90} exponential algal growth models are 0.81, 0.90, and 0.92 (Table S18), respectively, indicating that the time series data included in growth rate models exhibit exponential growth. The algal doubling time (T_d) is derived from the best-fit exponential growth rate (Table S18).

Mineral dissolution rates were determined for the mineral-bearing systems which showed enhanced algal growth relative to the Fe-depleted treatment, namely, the Fo^{90}-bearing experiment. Fo^{90} dissolution rates in biotic and abiotic experiments were determined from best-fit linear models ($R^2 = 0.96$) fit to Si release over time, which behaved as a conservative element as discussed above. Si concentrations are normalized to total surface area based on mineral mass and calculated specific surface area (0.118 m^{-2} g^{-1}) (Table S24) to yield linear dissolution rates reported in mol Si m^{-2} s^{-1}. The initial concentrations of Mg (20.3 μM) and Si (7.7 μM) within the growth medium were subtracted from the Fo^{90} dissolution data prior to calculating the Mg/Si ratio (Fig. 5).

***Pedobacter* isolation and characterization.** Bacterial isolation was performed via spreading coculture aliquots on plates containing NA-Fe M1 medium amended with 1% M1P. M1P photosynthate was prepared from an exponential-phase *C. brevispina* coculture maintained on Fe-EDTA M1 medium and centrifuged at 40,905 rcf for 10 min at 10°C. The supernatant was then filtered with glass fiber (GF/F) and 0.2-μm filters and added to the NA-Fe M1 medium. Plates of M1P were inoculated with 20 μl of *C. brevispina* coculture and incubated at 10°C; noninoculated plates were incubated in parallel. After 11 days of incubation, three colonies were selected from the M1P plates for purification through three rounds of plating. Purified colonies were inoculated into 2 ml of 10% R2A medium and incubated at 10°C on a shaker table at 150 rpm. All three isolate cultures were turbid after 17 days of incubation, at which time aliquots were preserved in 15% glycerol stocks stored at −80°C and prepared for DNA extraction. Nucleic acids were extracted (69), quantified using PicoGreen (Life Technologies) on a Spectromax Gemini microplate spectrofluorometer (Molecular Devices), and amplified by PCR using primers 27F (70) and −1391R (71). Amplicons were sequenced directly on a Prism 3730 DNA analyzer (Life Technologies) following agarose gel purification (Qiagen) using primer 27F.

Bacterial and archaeal DNA and MiSeq DNA sequencing. *C. brevispina* coculture was grown in Fe-EDTA M1 medium, and the M1P isolates were harvested in exponential-phase growth by centrifugation (1 ml, 5 min, 14,000 rpm) to isolate cells for 16S rRNA gene sequence analysis from the bacterial and potentially the archaeal fraction of the coculture. Nucleic acids were extracted using an enzymatic lysis and RNase digestion protocol, followed by phenol-chloroform-isoamyl alcohol purification and DNA precipitation using sodium acetate and ethanol (69). Extracts resuspended in 10 mM Tris-Cl were quantified by fluorescence with PicoGreen (Life Technologies) on a Spectramax Gemini microplate spectrofluorometer (Molecular Dynamics).

The amplicon library and DNA sequencing were prepared and performed at MR DNA (Shallowater, TX, USA) for MiSeq Illumina sequencing. Briefly, the v4 region of the 16S rRNA gene targeting bacteria and archaea was amplified (coculture primers 515F+barcode–806R and isolate primer Bact27F) (72) using a HotStart *Taq* Plus master mix kit (Qiagen, USA), purified using Ampure XP beads, and then prepared for MiSeq sequencing (paired end, 2 × 250 bp) in accordance with the manufacturer's guidelines. The sequence data were processed through the MR DNA processing pipeline.

16S rRNA gene data analysis. The paired-end reads were merged using the make.contigs command, part of the Mothur suite of tools. MiSeq SOP (73) was then adopted for sequence data screening, aligning, and clustering. Seed alignment and taxonomy files provided by the SILVA rRNA database project (www.arb-silva.de), Silva.seed_v128.align and silva.seed_v128.tax, were used for all reference alignment and taxonomic assignment. Chimera vsearch was used to identify chimeras in which 762 sequences were detected and removed. Sequences with ambiguities were removed, as were all sequences with >6 homopolymers and sequences with between 240 and 265 bases. The final coculture data set contained 55,342 sequences that fell into 137 operational taxonomic units (OTUs) defined at a distance of 0.03 (57 OTUs were singletons and doubletons). Plotted data are OTUs of greater than 1%, with all OTUs less than 1% binned as "other" (Fig. 3).

Accession number(s). The iTag FASTQ data for the coculture were submitted to the GenBank Sequence Read Archive under BioProject ID PRJNA427065, BioSample accession numbers SAMN08219688 to SAMN08219690, and SRA accession number SRP127719. The *Pedobacter* isolate 16S rRNA gene sequence GenBank accession number is MG692745.

SUPPLEMENTAL MATERIAL

Supplemental material for this article may be found at https://doi.org/10.1128/AEM.02322-17.

SUPPLEMENTAL FILE 1, PDF file, 1.6 MB.

ACKNOWLEDGMENTS

Funding for this work was provided by NASA grants NNX14AN24A and NNX17AF49G.

We thank M. Higham for help with 16S rRNA gene analyses, L. Bishop for work with the bacterial isolation, and Y. Teng for assistance with ICP-MS analyses and data processing. Many thanks to P. Sbraccia and T. Bamisile for their assistance in the lab, J. Batista for her insight on algal culture growth, and S. Gainey for his help with Fe(III) smectite syntheses. We also acknowledge thoughtful reviews from one AEM Editorial Board member and one anonymous reviewer that greatly strengthened this work.

REFERENCES

1. Warren SG. 1984. Impurities in snow: effects on albedo and snowmelt. Ann Glaciol 5:177–179. https://doi.org/10.3189/1984AoG5-1-177-179.
2. Benning LG, Anesio AM, Lutz S, Tranter M. 2014. Biological impact on Greenland's albedo. Nat Geosci 7:691–691. https://doi.org/10.1038/ngeo2260.
3. Lutz S, Anesio AM, Raiswell R, Edwards A, Newton RJ, Gill F, Benning LG. 2016. The biogeography of red snow microbiomes and their role in melting arctic glaciers. Nat Commun 7:11968. https://doi.org/10.1038/ncomms11968.
4. Yallop ML, Anesio AM, Perkins RG, Cook J, Telling J, Fagan D, MacFarlane J, Stibal M, Barker G, Bellas C. 2012. Photophysiology and albedo-changing potential of the ice algal community on the surface of the Greenland ice sheet. ISME J 6:2302–2313. https://doi.org/10.1038/ismej.2012.107.
5. Müller T, Bleiß W, Martin C-D, Rogaschewski S, Fuhr G. 1998. Snow algae from northwest Svalbard: their identification, distribution, pigment and nutrient content. Polar Biol 20:14–32. https://doi.org/10.1007/s003000050272.
6. Hoham RW, Berman JD, Rogers HS, Felio JH, Ryba JB, Miller PR. 2006. Two new species of green snow algae from Upstate New York, Chloromonas chenangoensis sp. nov. and Chloromonas tughillensis sp. nov (Volvocales, Chlorophyceae) and the effects of light on their life cycle development. Phycologia 45:319–330. https://doi.org/10.2216/04-103.1.
7. Hoham R, Duval B. 2001. Microbial ecology of snow and freshwater ice with emphasis on snow algae, p 168–215. *In* Jones HG, Pomeroy JW, Walker DA, Hoham RW (ed), Snow ecology: an interdisciplinary examination of snow-covered ecosystems. Cambridge Univesity Press, Cambridge, United Kingdom.
8. Hoham RW, Ling H. 2000. Snow algae: the effects of chemical and physical factors on their life cycles and populations, p 131–145. *In* Seckbach J (ed), Journey to diverse microbial worlds, vol 2. Springer, Dordrecht, The Netherlands.
9. Happey-Wood CM. 1988. Ecology of freshwater planktonic green algae, p 175–226. *In* Sandgren CD (ed), Growth and reproductive strategies of freshwater phytoplankton, 1st ed. Cambridge University Press, New York, NY.
10. Cook JM, Hodson AJ, Taggart AJ, Mernild SH, Tranter M. 2017. A predictive model for the spectral "bioalbedo" of snow. J Geophys Res Earth Surf 122:434–454. https://doi.org/10.1002/2016JF003932.
11. Ganey GQ, Loso MG, Burgess AB, Dial RJ. 2017. The role of microbes in snowmelt and radiative forcing on an Alaskan icefield. Nat Geosci 10:754–759. https://doi.org/10.1038/ngeo3027.
12. Hamilton TL, Havig J. 2017. Primary productivity of snow algae communities on stratovolcanoes of the Pacific Northwest. Geobiology 15:280–295. https://doi.org/10.1111/gbi.12219.
13. Tazaki K, Fyfe WS, Iizumi S, Sampei Y, Watanabe H, Goto M, Miyake Y, Noda S. 1994. Clay aerosols and arctic ice algae. Clays Clay Miner 42:402–408. https://doi.org/10.1346/CCMN.1994.0420404.
14. Lutz-Meindl U, Lutz C. 2006. Analysis of element accumulation in cell wall attached and intracellular particles of snow algae by EELS and ESI. Micron 37:452–458. https://doi.org/10.1016/j.micron.2005.11.004.
15. Schoffman H, Lis H, Shaked Y, Keren N. 2016. Iron-nutrient interactions within phytoplankton. Front Plant Sci 7:1223. https://doi.org/10.3389/fpls.2016.01223.
16. Geider RJ, La Roche J. 1994. The role of iron in phytoplankton photosynthesis, and the potential for iron-limitation of primary productivity in the sea. Photosynth Res 39:275–301. https://doi.org/10.1007/BF00014588.
17. Boyd RW, Watson AJ, Law CS, Abraham ER. 2000. A mesoscale phytoplankton bloom in the polar Southern Ocean stimulated by iron fertilization. Nature 407:695. https://doi.org/10.1038/35037500.
18. Price N, Ahner B, Morel F. 1994. The equatorial Pacific Ocean: grazer-controlled phytoplankton populations in an iron-limited ecosystem. Limnol Oceanogr 39:520–534. https://doi.org/10.4319/lo.1994.39.3.0520.
19. North RL, Guildford SJ, Smith REH, Havens SM, Twiss MR. 2007. Evidence for phosphorus, nitrogen, and iron colimitation of phytoplankton communities in Lake Erie. Limnol Oceanogr 52:315–328. https://doi.org/10.4319/lo.2007.52.1.0315.
20. Kouzuma A, Watanabe K. 2015. Exploring the potential of algae/bacteria interactions. Curr Opin Biotech 33:125–129. https://doi.org/10.1016/j.copbio.2015.02.007.
21. Kazamia E, Czesnick H, Nguyen TTV, Croft MT, Sherwood E, Sasso S, Hodson SJ, Warren MJ, Smith AG. 2012. Mutualistic interactions between vitamin B12-dependent algae and heterotrophic bacteria exhibit regulation. Environ Microbiol 14:1466–1476. https://doi.org/10.1111/j.1462-2920.2012.02733.x.
22. Amin SA, Hmelo LR, van Tol HM, Durham BP, Carlson LT, Heal KR, Morales RL, Berthiaume CT, Parker MS, Djunaedi B, Ingalls AE, Parsek MR, Moran MA, Armbrust EV. 2015. Interaction and signalling between a cosmopolitan phytoplankton and associated bacteria. Nature 522:98–101. https://doi.org/10.1038/nature14488.
23. Keshtacher-Liebso E, Hadar Y, Chen Y. 1995. Oligotrophic bacteria enhance algal growth under iron-deficient conditions. Appl Environ Microbiol 61:2439–2441.
24. Amin SA, Green DH, Hart MC, Kupper FC, Sunda WG, Carrano CJ. 2009. Photolysis of iron-siderophore chelates promotes bacterial-algal mutualism. Proc Natl Acad Sci U S A 106:17071–17076. https://doi.org/10.1073/pnas.0905512106.
25. Rogers JR, Bennett PC. 2004. Mineral stimulation of subsurface microorganisms: release of limiting nutrients from silicates. Chem Geol 203:91–108. https://doi.org/10.1016/j.chemgeo.2003.09.001.
26. Suzuki I. 2001. Microbial leaching of metals from sulfide minerals. Biotech Adv 19:119–132. https://doi.org/10.1016/S0734-9750(01)00053-2.
27. Song W, Ogawa N, Oguchi CT, Hatta T, Matsukura Y. 2007. Effect of *Bacillus subtilis* on granite weathering: a laboratory experiment. Catena 70:275–281. https://doi.org/10.1016/j.catena.2006.09.003.
28. Hutchens E. 2009. Microbial selectivity on mineral surfaces: possible implications for weathering processes. Fungal Biol Rev 23:115–121. https://doi.org/10.1016/j.fbr.2009.10.002.
29. Hutchens E, Valsami-Jones E, Harouiya N, Charat C, Oelkers EH, McEldoney S. 2006. An experimental investigation of the effect of *Bacillus megaterium* on apatite dissolution. Geomicrobiol J 23:177–182. https://doi.org/10.1080/01490450600599239.
30. Braun V, Hantke K. 2011. Recent insights into iron import by bacteria. Curr Opin Chem Biol 15:328–334. https://doi.org/10.1016/j.cbpa.2011.01.005.
31. Crowley D, Wang Y, Reid C, Szaniszlo P. 1991. Mechanisms of iron acquisition from siderophores by microorganisms and plants. Plant Soil 130:179–198. https://doi.org/10.1007/BF00011873.
32. Uroz S, Calvaruso C, Turpault MP, Sarniguet A, de Boer W, Leveau JHJ, Frey-Klett P. 2009. Efficient mineral weathering is a distinctive functional trait of the bacterial genus Collimonas. Soil Biol Biochem 41:2178–2186. https://doi.org/10.1016/j.soilbio.2009.07.031.
33. Bennett P, Rogers J, Choi W, Hiebert F. 2001. Silicates, silicate weathering, and microbial ecology. Geomicrobiol J 18:3–19. https://doi.org/10.1080/01490450151079734.

34. Thomas WH, Duval B. 1995. Sierra Nevada, California, USA, snow algae: snow albedo changes, algal-bacterial interrelationships, and ultraviolet radiation effects. Arctic Alpine Res 27:389–399. https://doi.org/10.2307/1552032.
35. Eckhardt U, Buckhout TJ. 1998. Iron assimilation in Chlamydomonas reinhardtii involves ferric reduction and is similar to strategy I higher plants. J Exp Bot 49:1219–1226. https://doi.org/10.1093/jxb/49.324.1219.
36. Lynnes JA, Derzaph TL, Weger HG. 1998. Iron limitation results in induction of ferricyanide reductase and ferric chelate reductase activities in *Chlamydomonas reinhardtii*. Planta 204:360–365. https://doi.org/10.1007/s004250050267.
37. La Fontaine S, Quinn JM, Nakamoto SS, Page MD, Göhre V, Moseley JL, Kropat J, Merchant S. 2002. Copper-dependent iron assimilation pathway in the model photosynthetic eukaryote *Chlamydomonas reinhardtii*. Eukaryot Cell 1:736–757. https://doi.org/10.1128/EC.1.5.736-757.2002.
38. Quisel JD, Wykoff DD, Grossman AR. 1996. Biochemical characterization of the extracellular phosphatases produced by phosphorus-deprived *Chlamydomonas reinhardtii*. Plant Physiol 111:839–848. https://doi.org/10.1104/pp.111.3.839.
39. de Hostos EL, Togasaki RK, Grossman A. 1988. Purification and biosynthesis of a derepressible periplasmic arylsulfatase from *Chlamydomonas reinhardtii*. J Cell Biol 106:29–37. https://doi.org/10.1083/jcb.106.1.29.
40. Hoham RW, Roemer SC, Mullet JE. 1979. The life history and ecology of the snow alga *Chloromonas brevispina* comb. nov. (Chlorophyta, Volvocales). Phycologia 18:55–70. https://doi.org/10.2216/i0031-8884-18-1-55.1.
41. Fournelle J. 2009. Notes on some crystals of San Carlos olivine and EPMA standards, abstr V31E-2009. Fall Meet 2009 Am Geophys Union. American Geophysical Union, San Franscisco, CA.
42. Pokrovsky OS, Schott J. 2000. Kinetics and mechanism of forsterite dissolution at 25 °C and pH from 1 to 12. Geochim Cosmochim Acta 64:3313–3325. https://doi.org/10.1016/S0016-7037(00)00434-8.
43. Hoham RW. 1992. Environmental influences on snow algal microbes, p 78–83. *In* Proceedings of the Sixtieth Annual Western Snow Conference, Jackson Hole, WY.
44. Hoham RW, Mohn WW. 1985. The optimum pH of four strains of acidophilic snow algae in the genus *Chloromonas* (*chlorophyta*) and possible effects of acid precipitation. J Phycol 21:603–609. https://doi.org/10.1111/j.0022-3646.1985.00603.x.
45. Lucas SB, St-Onge M. 1998. Geology of the Precambrian Superior and Grenville Provinces and Precambian fossils in North America. *In* Ingles OE (ed), Geology of Canada, vol 7. Geological Survey of Canada, Ottawa, Canada.
46. Lutz S, Anesio AM, Edwards A, Benning LG. 2017. Linking microbial diversity and functionality of arctic glacial surface habitats. Environ Microbiol 19:551–565. https://doi.org/10.1111/1462-2920.13494.
47. Liu Y, Yao T, Kang S, Jiao N, Zeng Y, Shi Y, Luo T, Jing Z, Huang S. 2006. Seasonal variation of snow microbial community structure in the East Rongbuk Glacier, Mt. Everest. Chin Sci Bull 51:1476–1486.
48. Cameron KA, Hagedorn B, Dieser M, Christner BC, Choquette K, Sletten R, Crump B, Kellogg C, Junge K. 2015. Diversity and potential sources of microbiota associated with snow on western portions of the Greenland Ice Sheet. Environ Microbiol 17:594–609. https://doi.org/10.1111/1462-2920.12446.
49. Lopatina A, Krylenkov V, Severinov K. 2013. Activity and bacterial diversity of snow around Russian Antarctic stations. Res Microbiol 164:949–958. https://doi.org/10.1016/j.resmic.2013.08.005.
50. Hisakawa N, Quistad SD, Hester ER, Martynova D, Maughan H, Sala E, Gavrilo MV, Rohwer F. 2015. Metagenomic and satellite analyses of red snow in the Russian Arctic. PeerJ 3:e1491. https://doi.org/10.7717/peerj.1491.
51. Zhang S, Hou S, Qin X, Du W, Liang F, Li Z. 2015. Preliminary study on effects of glacial retreat on the dominant glacial snow bacteria in Laohugou Glacier No. 12. Geomicrobiol J 32:113–118. https://doi.org/10.1080/01490451.2014.929761.
52. Leveau JHJ, Uroz S, De Boer W. 2010. The bacterial genus *Collimonas*: mycophagy, weathering and other adaptive solutions to life in oligotrophic soil environments. Environ Microbiol 12:281–292. https://doi.org/10.1111/j.1462-2920.2009.02010.x.
53. Lapanje A, Wimmersberger C, Furrer G, Brunner I, Frey B. 2012. Pattern of elemental release during the granite dissolution can be changed by aerobic heterotrophic bacterial strains isolated from Damma Glacier (Central Alps) deglaciated granite sand. Microb Ecol 63:865–882. https://doi.org/10.1007/s00248-011-9976-7.
54. Vasil ML, Ochsner UA. 1999. The response of *Pseudomonas aeruginosa* to iron: genetics, biochemistry and virulence. Mol Microbiol 34:399–413. https://doi.org/10.1046/j.1365-2958.1999.01586.x.
55. Loper JE, Henkels MD. 1997. Availability of iron to *Pseudomonas fluorescens* in rhizosphere and bulk soil evaluated with an ice nucleation reporter gene. Appl Environ Microbiol 63:99–105.
56. Cornelis P. 2010. Iron uptake and metabolism in pseudomonads. Appl Microbiol Biotechnol 86:1637–1645. https://doi.org/10.1007/s00253-010-2550-2.
57. Ochsner UA, Wilderman PJ, Vasil AI, Vasil ML. 2002. GeneChip® expression analysis of the iron starvation response in *Pseudomonas aeruginosa*: identification of novel pyoverdine biosynthesis genes. Mol Microbiol 45:1277–1287. https://doi.org/10.1046/j.1365-2958.2002.03084.x.
58. Yang L, Barken KB, Skindersoe ME, Christensen AB, Givskov M, Tolker-Nielsen T. 2007. Effects of iron on DNA release and biofilm development by *Pseudomonas aeruginosa*. Microbiology 153:1318–1328. https://doi.org/10.1099/mic.0.2006/004911-0.
59. Banin E, Vasil ML, Greenberg EP. 2005. Iron and *Pseudomonas aeruginosa* biofilm formation. Proc Natl Acad Sci U S A 102:11076–11081. https://doi.org/10.1073/pnas.0504266102.
60. Männistö MK, Häggblom MM. 2006. Characterization of psychrotolerant heterotrophic bacteria from Finnish Lapland. Syst Appl Microbiol 29:229–243. https://doi.org/10.1016/j.syapm.2005.09.001.
61. Pokrovsky OS, Schott J. 2000. Forsterite surface composition in aqueous solutions: a combined potentiometric, electrokinetic, and spectroscopic approach. Geochim Cosmochim Acta 64:3299–3312. https://doi.org/10.1016/S0016-7037(00)00435-X.
62. Olsen AA, Rimstidt DJ. 2008. Oxalate-promoted forsterite dissolution at low pH. Geochim Cosmochim Acta 72:1758–1766. https://doi.org/10.1016/j.gca.2007.12.026.
63. Schwertmann U, Cornell RM. 2000. Iron oxides in the laboratory: preparation and characterization, 2nd ed. Wiley-VCH, Weinheim, Germany.
64. Mizutani T, Fukushima Y, Okada A, Kamigaito O, Kobayashi T. 1991. Synthesis of 1:1 and 2:1 iron phyllosilicates and characterization of their iron state by Mössbauer spectroscopy. Clays Clay Miner 39:381–386. https://doi.org/10.1346/CCMN.1991.0390407.
65. Bacelar-Nicolau P, Johnson DB. 1999. Leaching of pyrite by acidophilic heterotrophic iron-oxidizing bacteria in pure and mixed cultures. Appl Environ Microbiol 65:585–590.
66. Jenneman GE, McInerney MJ, Crocker ME, Knapp RM. 1986. Effect of sterilization by dry heat or autoclaving on bacterial penetration through Berea sandstone. Appl Environ Microbiol 51:39–43.
67. Brantley SL, Mellott NP. 2000. Surface area and porosity of primary silicate minerals. Am Mineral 85:1767. https://doi.org/10.2138/am-2000-11-1220.
68. Porter KG, Feig YS. 1980. The use of DAPI for identifying and counting aquatic microflora1. Limnol Oceanogr 25:943–948. https://doi.org/10.4319/lo.1980.25.5.0943.
69. Massana R, Murray AE, Preston CM, DeLong EF. 1997. Vertical distribution and phylogenetic characterization of marine planktonic Archaea in the Santa Barbara Channel. Appl Environ Microbiol 63:50–56.
70. Lane DJ. 1991. 16S/23S rRNA sequencing, p 115–175. *In* Stackebrandt E, Goodfellow M (ed), Nucleic acid techniques in bacterial systematics. Wiley, New York, NY.
71. Turner S, Pryer KM, Miao VF, Palmer JD. 1999. Investigating deep phylogenetic relationships among cyanobacteria and plastids by small subunit rRNA sequence analysis. J Eukaryot Microbiol 46:327–338. https://doi.org/10.1111/j.1550-7408.1999.tb04612.x.
72. Caporaso JG, Lauber CL, Walters WA, Berg-Lyons D, Lozupone CA, Turnbaugh PJ, Fierer N, Knight R. 2011. Global patterns of 16S rRNA diversity at a depth of millions of sequences per sample. Proc Natl Acad Sci U S A 108:4516–4522. https://doi.org/10.1073/pnas.1000080107.
73. Kozich JJ, Westcott SL, Baxter NT, Highlander SK, Schloss PD. 2013. Development of a dual-index sequencing strategy and curation pipeline for analyzing amplicon sequence data on the MiSeq Illumina sequencing platform. Appl Environ Microbiol 79:5112–5120. https://doi.org/10.1128/AEM.01043-13.